Earth Surf. Dynam. Discuss., https://doi.org/10.5194/esurf-2018-63
Manuscript under review for journal Earth Surf. Dynam.
Discussion started: 11 September 2018

Earth Surface Dynamics Discussions
Open Access
EGU

Estimating lateral moraine sediment supply to a debris-covered glacier in the Himalaya

Teun van Woerkom[1], Jakob F. Steiner[1], Philip D.A. Kraaijenbrink[1], Evan S. Miles[2], and Walter W. Immerzeel[1]

[1]Utrecht University, Department of Physical Geography, PO Box 80115, Utrecht, The Netherlands
[2]School of Geography, University of Leeds, Leeds, UK

Correspondence: Jakob F. Steiner (j.f.steiner@uu.nl)

Abstract. Debris-covered glacier tongues in the Himalaya play an important role in the high-altitude water cycle. The thickness of the debris layer is a key control of the melt rate of those tongues, yet little is known about the relative importance of the three potential sources of debris supply to those glaciers: the headwalls, the glacier bed or the lateral moraines. In this study we hypothesize that erosion from the lateral moraines is a significant debris supply to the debris-covered tongues, in particular when the tongue is disconnected from the headwall due to glacier downwasting. To test this hypothesis eight high-resolution and highly accurate digital elevation models for the lateral moraines of the debris-covered Lirung glacier in Nepal derived from an unmanned aerial vehicle between May 2013 and April 2018 are used. The analysis shows that the lateral moraines erode at an average rate of 0.31 ± 0.26 m yr^{-1} during this period driven by different erosion processes. There is also a higher erosion rate observed in the monsoon season (0.42 m yr^{-1}) than in the dry season (0.25 m yr^{-1}). In addition the loose lower parts of the lateral moraines erode at a faster rate during both seasons. These erosion rates translate into an annual increase in debris thickness ranging from 0.17 m yr^{-1} when the eroded material is distributed over the entire glacier to 0.29 m yr^{-1} in case the material is deposited in a narrow runout zone. It is concluded that the lateral moraines provide an important source of surface debris for glaciers in an advanced state of mass loss, and the source needs to be incorporated into models of glacier evolution. Further research should focus on how large this negative feedback is in controlling the melt of the tongues and a better understanding of the redistribution of debris on the tongue is therefore required.

1 Introduction

Glaciers cover approximately 100000 km^2 in High Mountain Asia (HMA) and as such constitute an important water storage of the region (Pfeffer et al., 2014; Immerzeel et al., 2010). The glaciers are likely to melt rapidly in the future with projections ranging from a total mass loss of 36% to 64% in the coming century depending on the climate scenario (Kraaijenbrink et al., 2017). While the whole HMA has experienced an overall glacier mass and area loss in recent decades, the changes have been found to be variable in space (Bolch et al., 2012; Kääb et al., 2012; Brun et al., 2017). Apart from differences in climate, the presence of debris with variable thickness on the glacier tongues plays an important role to explain this spatial heterogeneity (Scherler et al., 2011; Gardelle et al., 2012; Kääb et al., 2012).

Earth Surf. Dynam. Discuss., https://doi.org/10.5194/esurf-2018-63
Manuscript under review for journal Earth Surf. Dynam.
Discussion started: 11 September 2018

Although debris-covered glaciers (DCGs) only constitute 11% of the total glacier area, 30% of the ice mass below the equilibrium line altitude (ELA) is covered in debris (Kraaijenbrink et al., 2017). While a thin debris cover increases melt because it decreases albedo, debris beyond a couple of centimeters in thickness inhibits melt (Østrem, 1959). The surface of a DCG is often characterized by ice cliffs and supraglacial ponds, which result in high local melt rates (Immerzeel et al., 2014a; Steiner et al., 2015; Thompson et al., 2016; Miles et al., 2017a). Knowledge about actual debris thickness is limited to few field observations (Nicholson and Benn, 2006; Ragettli et al., 2015; McCarthy et al., 2017) and attempts to derive it from thermal bands of satellite imagery (Mihalcea et al., 2008; Foster et al., 2012; Rounce and McKinney, 2014; Schauwecker et al., 2015; Rounce et al., 2018). Several studies suggest that glaciers with prolonged periods of negative mass balance are associated with an increase in debris cover (Deline, 2005; Mihalcea et al., 2006; Stokes et al., 2007; Shukla et al., 2009; Kirkbride and Deline, 2013; Gibson et al., 2017b). Glaciers that have a neutral or positive mass balance, such as in the Karakoram in Pakistan, do not show any positive trends in debris-covered area (Herreid et al., 2015).

Not only is the debris-covered area variable, but the thickness also changes over time. A recent study on the Baltoro glacier in Pakistan suggested that debris thickness changes at rates of multiple centimeters per year with a maximum of 30 cm yr^{-1} near the snout (Gibson et al., 2017a).

The source of supraglacial debris has been studied for decades (Reheis, 1975; Boulton, 1978). Three potential sources of supraglacial debris can be distinguished: basal erosion, bordering headwalls and lateral moraines (Figure 1A). The relative contribution of these sources is variable, but generally depends on the amount and intensity of the precipitation, the glacier size, and the erodibility of the bedrock and sediments (Benn and Ballantyne, 1994; Benn and Owen, 2002). In HMA, basal erosion (Figure 1A-a) is likely only of limited relative importance, as the erosion processes on the steep headwalls and lateral moraines are highly active (Benn and Ballantyne, 1994; Benn and Owen, 2002). Bordering headwalls have been observed to transport debris to the glacier via rockfall, rock avalanches and landslides as primary transporting processes (Figure 1A-b). These periodic events can be triggered by processes such as extreme rainfall or seismic events, and are known to increase due to glacier melt and downwasting of the surface resulting in debuttressing and exposure of unsupported strata (Soldati et al., 2004; Deline et al., 2014).

Generally, long-term headwall erosion rates are in the order of 1 mm yr^{-1} (Heimsath and McGlynn, 2008). However actual mass deposited on the glacier surface are more difficult to determine and vary from glacier to glacier, depending on its exposure to headwalls and geologic conditions. The reworking of these deposits on the glacier surface, as a result of local hillslope geomorphology, surface melt, glacier flow and englacial processes, may lead to small-scale variations in debris cover as found in the Himalaya. In contrast to transport from the headwalls, which deposits material on specific locations, processes on lateral moraines can result in a much more spatially uniform debris supply to the glacier (Figure 1A-c). Lateral moraines typically have a gullied upper part, where debris flow is the main transport process (Curry et al., 2006) (Figure 1B-c1). Most of these flows are released due to rainfall saturation, but the melt of buried ice cores can contribute as well (Ballantyne, 2002). The oversteepened upper parts may also be susceptible to rockfall (Lukas et al., 2012) (Figure 1B-c2). Below the upper parts, material on talus slopes is reworked by small landslides, debris flows, snow avalanches and solifluction (Figure 1B-c3). The transport processes on the moraines are most active directly after deglaciation (Ballantyne and Matthews, 1982).

Earth Surf. Dynam. Discuss., https://doi.org/10.5194/esurf-2018-63
Manuscript under review for journal Earth Surf. Dynam.
Discussion started: 11 September 2018

Although it is generally assumed that headwalls are the main source of debris, we hypothesize that further down-glacier the supply from lateral moraines becomes an important source of debris, particularly for stagnating glacier tongues whose headwalls are disconnected from the actual tongue due to glacier retreat and downwasting. In such cases rockfall and avalanches from the headwalls no longer reach the tongue (Figure 3B and 3C). Material deposited below the ELA is furthermore only advected on the glacier surface rather than transported along an englacial pathway. Estimated erosion rates from the lateral moraines range from 49 to 151 mm yr^{-1} for the European Alps (Curry et al., 2006) and 3 to 169 mm yr^{-1} for Norwegian field sites (Curry et al., 2006). On glaciers in the study area (Langtang Valley in Nepal) a supply rate of 0.4 – 31 mm yr^{-1} (Watanabe et al., 1998) was previously found. However these values are averages over a much larger time span (<550 years versus <247 years for studies in Norway and <79 for the Alps, (Curry et al., 2006)) and include source areas beyond the moraines. These rates are however all much higher than headwall erosion rates and all eroded material is deposited on debris cones on the tongue.

Previous studies only reported glacier-averaged erosion rates, although it is likely that the rates are spatially variable. In this study we use multi-annual, high-resolution orthomosaics and digital elevation models (DEM) acquired using an unmanned aerial vehicle to quantify erosion rates of the lateral moraines of a DCG in Nepal. We attempt to explain the spatio-temporal variability and sediment transport processes using the terrain morphology and prevailing seasonal climates. Finally, we assess how important erosion from lateral moraines is in the formation of Himalayan DCGs.

2 Study area

The research was conducted on Lirung Glacier (28.23 N, 85.56 E), which is located in the Langtang Valley in the Nepalese Himalaya (Figure 2B). The glacier has a southern aspect, steep headwalls near the mountain crest and an almost flat terminus. The lower part of the glacier is covered entirely in debris (Figure 3) and has been subject to strong downwasting in recent decades (Immerzeel et al., 2014a; Nuimura et al., 2017). The study area is located between 3900 and 4400 m a.m.s.l. In this section the moraine (Figure 2C, orange lines) is disconnected from the upper slopes, and up to 5 m above the surrounding non-glacial topography. The climate in the region is dominated by the monsoon, with a wet season between June and September in which 70% of the annual precipitation falls. During the dry season between November and May, considerably less precipitation reaches the area, and falls mostly as snow (Immerzeel et al., 2014b).

3 Data and methods

3.1 Field data

Our observations of the lateral moraines of Lirung Glacier span 2013 to 2018, consisting of co-registered orthomosaics (0.1 m resolution) and DEMs (0.2 m) derived from multiple UAV flights with an optical camera (for details regarding measurements, processing and data quality see Kraaijenbrink et al., 2016). Details about the mapped part of the glacier for each UAV cam-

Earth Surf. Dynam. Discuss., https://doi.org/10.5194/esurf-2018-63
Manuscript under review for journal Earth Surf. Dynam.
Discussion started: 11 September 2018

paign are provided in Table 1. The mutually overlapping area of all datasets covers 1.5 km^2 of the glacier tongue including the moraines.

Precipitation data was available from the meteorological station at Kyanjing village (28.21 N, 85.57 E) about 1.3 km south of the glacier in 2013. As data gaps are present between 2015 and 2018 for the Kyanjing station, the meteorological station in Langshisha (N 28.20, E 85.67) about 13 km south-east of the glacier was used for the remainder of the period. Both rainfall intensities and the cumulative rainfall between any two UAV time slices were analyzed.

3.2 Deriving change in elevation

The DEMs were used to calculate elevation differences between time steps. The difference in elevation between two timesteps was assumed equal to the amount of sediment transport, assuming that no melting ice core exists in the moraine. Two preprocessing steps were taken. First, vegetated areas were selected using a maximum likelihood supervised classification applied to the orthomosaic and masked out of the DEMs, to ensure that the moraine elevation changes represent real change. Second, in the case of a large elevation change in terrain that is assumed to be stable, it is likely that this offset also influences elevation changes on the moraine itself. Therefore the DEMs were corrected for elevation changes in off-moraine and off-glacier terrain. To not bias the result towards possible errors in the DEM as well as extreme events, we removed the outliers outside the 10-90 percentile range (Table 2).

3.3 Analysis of surface properties

The orthomosaics were analyzed visually to examine patterns of erosion and deposition, and compared against elevation differences. Furthermore, the displacement, slope and roughness of the lateral moraines were derived from the DEMs. We employed the COSI-Corr software for cross-correlation feature tracking to calculate the displacement of debris on the lateral moraines (Leprince et al., 2007; Kraaijenbrink et al., 2016). As this software focuses more on block movement than on individual clast displacement (Leprince et al., 2007), correlating displacement with elevation change gives insight in slower slope processes such as creep or solifluction, which often occur on a scale large enough to be detected by COSI-Corr. Fast flows and slides that may happen within a few minutes are also captured as movement in the same signal. Slope maps are created directly from the DEM. The last derivative dataset, surface roughness, was extracted from the DEM. Following Nield et al. (2013), the roughness length z_0 [m] was derived by

$$\ln(z_0) = 0.65 + 1.37 \ln(\sigma_z) \tag{1}$$

with σ_z defined as the standard deviation of a 5×5 m window of a detrended DEM. Although the window size greatly influences the roughness, a window of 25 m^2 is suitable for this approach (Miles et al., 2017b). For each window a high roughness value indicates larger topographic variation, such as boulders, while a small value indicates a more homogeneous surface (Miles et al., 2017b).

Earth Surf. Dynam. Discuss., https://doi.org/10.5194/esurf-2018-63
Manuscript under review for journal Earth Surf. Dynam.
Discussion started: 11 September 2018

3.4 Moraine delineation

The DEM and orthomosaic, as well as their derivatives, were used to delineate the lateral moraines and divide them into zones with comparable characteristics. The moraine base is often characterized by a break in slope (Figure 3, Figure 4A). Furthermore, a hillshade with a hummocky appearance is an indicator for subdebris ice (Lukas et al., 2012), and is often used to define the lower moraine boundary. Within the lateral moraine two main zones were distinguished: an intensively gullied upper part of firm material and a lower part (Curry et al., 2006) that consists of loose material (Figure 3, Figure 4A). Although not distinguishable everywhere, a zone with fine material was detected directly below the gullied upper part, accompanied by a very low roughness (Figure 4C). The smoothness is also visible on the orthomosaic. We interpret this as the depositional zones of the gullies upslope, and refer to it hereafter as 'washout zone'.

3.5 Runout model

To investigate the importance of the lateral moraines as a source for supraglacial debris, we used a simple model to calculate how far moraine material can travel onto the glacier. The model is based on the reach angle principle. The reach angle is the angle between the origin and maximum reach of a mass movement, and has a range between 3° and 45° (Evans and Hungr, 1993). For debris flows the reach angle is generally between 26° and 34° (De Haas et al., 2015). These variations are mainly caused by differences in processes, but the volume of the mass wasting is also important (Dai and Lee, 2002). Taking both process and volume into account, minimum reach angles for rockfall, shallow slides and debris flows are found to be 33° (with a volume of 100 - 1000 m^3), 23° (800 - 2000m^3), and 22° (800 - 2000m^3) respectively (Corominas et al., 2003). Reach angles decrease for values beyond these ranges, and increase for smaller volumes.
The runout length R_L (m) from the lower moraine boundary was calculated as

$$R_L = \frac{\Delta H}{\tan(\mathrm{R}_\alpha)} - M_w \tag{2}$$

where ΔH is the difference in elevation between start end location of deposition (m), R_α (°) is the reach angle (Figure 8A) and M_w is the planar moraine width (m). To derive the maximum runout length, it was assumed that the start location of the mass transport is at the moraine crest, though in reality they may start from anywhere inside the firm zone (Curry et al., 2006). As the minimum reach angles were used and since we assume the moraine crest as a starting point, the calculated runout length R_L indicates the furthest inward point on the glacier that debris can be transported to. Due to a decrease in mass movement velocity after the abrupt slope change on the glacier-moraine boundary, the amount of debris deposition is expected to be highest close to the moraine and will decrease rapidly with distance. To validate this estimated runout length, the actual runout length is determined by detecting depositional features such as debris flow lobes and tumbled rocks, and measuring their distance to the moraine edge.

Earth Surf. Dynam. Discuss., https://doi.org/10.5194/esurf-2018-63
Manuscript under review for journal Earth Surf. Dynam.
Discussion started: 11 September 2018

3.6 Clast analysis

Model results were validated by performing a clast analysis, which was conducted by investigating 70 individual samples of debris. For each of the locations on average 46 (σ = 25) clasts were analyzed. The roundness is determined based on the commonly used chart from Powers (1953), which results in a percentage of clasts for each sample that are angular or very angular (RA index). For 13 samples the axis length of each clast was measured, allowing us to determine the so called C_{40}, which is the 40th percentile ratio of short to long axes (c/a) in a sample. These indices are widely used to distinguish between actively transported clasts (low C_{40} and RA) and those that are mostly affected by weathering and reworking in rapid mass movement events (Lukas et al., 2013, high values). Moraine-derived debris is assumed to have already been transported by the ice, and therefore has lower RA values than headwall-derived debris, which is expected to be more dominant in the centre of the tongue. It has to be taken into account that both the C_{40} and RA indices decline down-glacier (Benn and Ballantyne, 1994) and that differences in lithology result in different index values (Lukas et al., 2013). However, the latter will be of minor importance as the debris catchment is relatively small and homogeneous in lithology (Macfarlane et al., 1992). If the lateral moraine indeed is an important source of debris, clast roundness is expected to decreases from the lateral moraine towards the glacier centre, as the influence of the lateral moraine diminishes and material transported from further up-glacier becomes dominant.

4 Results and discussion

4.1 Observed erosion rates

The mean elevation change rate of the non-vegetated moraine between May 2013 and April 2018 equals 0.31 m yr^{-1}, with a variability of 0.26 m yr^{-1} (Table 3). Most elevation change occurs in the lower loose part of the moraine, at a rate of approximately 0.35 m yr^{-1}. The upper firm part on average has a smaller erosion rate of 0.16 m yr^{-1}. In the same area denudation erosion rates up to only 0.03 m yr^{-1} are found (Watanabe et al., 1998). Both the inclusion of upper mountain slopes, rather than just focusing on lateral moraines and the fact that these are average rates for up to five centuries may explain the difference. Elevation change on other moraines that formed during more recent glaciations and mountain ranges that are generally less erosive than the Himalayas peaked at approximately 0.15 m yr^{-1} (Curry et al., 2006), with Ballantyne and Benn (1994) noting their rates between 0.01 and 0.02 m yr^{-1} to be minimum rates. The high erosion rates found are indicative for rapid surface change on steep lateral moraines above downwasted glacier tongues during the peak period of debris supply during deglaciation and debuttressing. The vertical accuracy of the dataset is determined by calculating DEM differences for off-glacier and off-moraine terrain between May and October 2013. Over an area of 1.6 km^2 the average deviation is 0.02 m yr^{-1} $\pm$0.33 m yr^{-1} (Immerzeel et al., 2014a), which is an acceptable error in comparison to the observed erosion rates.

Earth Surf. Dynam. Discuss., https://doi.org/10.5194/esurf-2018-63
Manuscript under review for journal Earth Surf. Dynam.
Discussion started: 11 September 2018

4.2 Erosion mechanisms and processes

Our data enables us to differentiate between different transport mechanisms, which can be divided in three main categories: erosion due to running water (entrainment and debris flows), larger mass movements (slumps or rockfall) and slower downslope processes (for example solifluction). Despite the overall stability of the firm moraine, the gullied topography indicates the importance of flow erosion processes. Debris flows and sediment loaded streams originate here mostly in the wet season, when there is frequent rainfall often with high intensity (Table 3). Often a patch of higher erosion is found just below the firm zone, as the break in slope causes the flows to plunge into the loose material below (Figure 5A). On the loose part, flow velocities decrease as a result of the shallower slope, resulting in deposition on the lower parts. Frequently observed grain diameters of > 40 cm in the loose zone indicate the importance of debris flows over water flows (Iverson, 1997), as debris flows, in contrast to water alone, are able to transport boulders of such a dimension. Distinct levees along a central flowpath and lobe-like features support this idea (Figure 5C). Nonetheless, many smaller channels show the importance of water flows for further reworking the sediment. The steep upper slopes are also susceptible to larger mass movements, such as the occurrence of slumps and tumbling rocks. These processes may be enhanced by oversteepening of the slope by the water flow processes, and cause locally high (>2 m) erosion rates (Figure 5A1). The slump toe is mostly still located on the moraine, where its loose material is susceptible to continued erosion in the years after the event. The lower part of the moraine is also eroded by water flow, but additionally moves downslope as a whole (Figure 5B). Although the contribution to surface lowering by slumping is unclear, the process does result in a steady debris supply to the glacier. With average surface velocities of 0.93 m yr^{-1}, and a 90^{th} percentile of 2.01 m yr^{-1}, the process is much faster than creep, which is in the order of cm yr^{-1} (Kirkby, 1967) and is in the range of movement through solifluction and of rock glaciers (Matsuoka, 2001; Frauenfelder et al., 2005). As permafrost can be found above 3500 m in the study region (Gruber et al., 2017), solifluction might be the main transport mechanism.

4.3 Temporal patterns in erosion

Moraine erosion occurred throughout the year, and a considerable difference was observed between the wet (0.42 m yr^{-1}) and dry (0.25 m yr^{-1}) season. For the firm part of the moraine, seasonal erosion values were highly variable (0.07 to 0.28 m yr^{-1}), but generally lower than erosion rates on the loose part of the moraine (0.25 to 0.6 m yr^{-1}). On both sections, erosion rates were higher in the wet seasons, which indicates the importance of water-driven erosion and slumping (Table 3).
The difference between the two seasons was caused by heavier precipitation during the summer months. Erosion processes were more active in the wet seasons than in the dry seasons, with erosion rates ranging from 0.34 to 0.52 m yr^{-1} and 0.17 to 0.36 m yr^{-1}, respectively, and total cumulative precipitation of 540 - 700 mm and 117 - 145 mm. The upper moraine experiences less change throughout the dry season, but is also more sensitive to precipitation changes as the seasonal differences in erosion rates are higher. During the dry season from 2016 to 2017, when erosion values were especially high, both the total precipitation as well as the intensity were considerably higher. In line with the larger negative elevation change that was observed on the firm part, gully erosion was observed after the wet season. Larger slumps and rockfall from the firm part were observed in both seasons, as they are mostly triggered by a single rainfall event rather than by continuous wetting. Deposition below the firm

part in the washout zone can be seen throughout the wet and dry season, which is also true for the sliding of the entire slope. Nonetheless, the rate of movement was much faster during the wet summer season. On the other hand, a larger loading and decrease of shear strength may also cause the moraine to shift down faster (Cai and Ugai, 2004). Although the exact process is yet unclear and needs further investigation, it is clear that this shift does contribute substantially to the downslope movement of moraine debris.

Beyond precipitation, freeze-thaw cycles could also play a role in driving erosion, with erosion increasing as moraine slopes warm up seasonally after the dry winter season and diurnally through the rest of the year.

4.4 Towards a conceptual lateral moraine erosion model

The steep intensely gullied firm part of the moraine had lower erosion values (0.16 m yr^{-1}) than the lower loose part (0.35 m yr^{-1}) (Figure 5). Although counterintuitive, this is in line with other studies that indicate that post-deglaciation the steep upper slopes get rapidly deprived from their loose sediment (Ballantyne, 2002; Curry et al., 2006). This would suggest higher erosion rates on the upper moraine part in the past, and this hypothesis is supported by the large amount of loose material below. Currently, erosion still occurs in these gullies albeit at a lower rate, as deposition features just below the firm part fill the gaps between the larger boulders and decrease the surface roughness locally (Figure 4C). A higher roughness causes water to become more concentrated in gullies, resulting in higher flow velocities and more erosion (Römkens et al., 2002). Finer grain deposits on the lower moraine makes debris more susceptible to water erosion in shallower slopes (van Rijn, 1984). An alternative explanation for high rates in the lower parts could be that in addition to surface erosion, larger sections of the moraine may slump as a unit. This may occur most commonly in close proximity of the glacier ice in areas of high mass loss, as the ice thins vertically but also recedes laterally (Figure 6A). These slump deposits may be identified on the moving glacier as positive surface elevation change due to the advection of a prominent zone (Figure 6B).

Erosion on the loose part of the moraine is related to moraine displacement in the wet season. In the wet season, when surface displacement rates were on average >1 m yr^{-1}, higher velocities coincide with a more negative elevation change (Figure 7). The displacements were caused by a slower slumping process, which moves down the moraine sediment as a block that is mostly active in the wet summer season. As these displacements were directly caused by a debris transport process, the moraine velocity is an indicator for erosion, instead of the other way around. The firm part of the moraine was approximately stable in both seasons. In the dry season, displacement rates were lower (< 1 m yr^{-1}) and do not show a correlation with elevation change, indicating a smaller importance of this process.

It is difficult to quantify the importance of fast processes such as debris flows, rockfall of individual large boulders and landslides on the moraine. However, as the latter two only occurred occasionally and covered a small area (width of maximum 25 m) their total contribution to the glacier is assumed to be small.

As there was no relation in the dry season between flow velocity and surface elevation change (Figure 7), other processes are important on the loose part of the moraine. No debris flows or landslides were detected on this part, hence it is most likely that erosion in the lower part was triggered by water and debris flow erosion that originated on the upper steep part.

Earth Surf. Dynam. Discuss., https://doi.org/10.5194/esurf-2018-63
Manuscript under review for journal Earth Surf. Dynam.
Discussion started: 11 September 2018

4.5 Debris distribution onto the glacier

The main processes (debris flow, shallow slides, rockfall) described above were included in the model to calculate on-glacier debris deposition.

Using a specific reach angle for each process, the maximum runout length on the glacier is 39.4 m for rockfall, 111.4 m for debris flow and 121.8 m for shallow slides (Figure 8B). The runout length is not equal along the glacier, as a result of differences in moraine elevation and the hummocky glacier surface (Figure 8C). The observed runout length has a maximum of 51.4 m, which suggests rockfall as the most important process, being closest to this value. As rockfall was not observed to be the most important process on the moraine, this difference also indicates that debris flows and small slumps possibly occurred with smaller runout lengths than modelled. There are two possible explanations for this. First, many mass movements might have a smaller volume than the 800-2000 m^3 range used in the calculation, which reduces the runout length (Corominas et al., 2003; Rickenmann, 2005). Second, the rough surface on the glacier obstructs the runout path and decreases runout length substantially (Corominas et al., 2003; Miles et al., 2017b). Using a smaller volume (<800 m^3) and an obstructed path, the reach angle of debris flows and shallow slides decreases to 30°, which results in a maximum runout length of 56.4 m, much closer to the observed length of 51.3 m (Figure 8B). Nonetheless, both the calculated and measured runout lengths indicate that debris from the moraine cannot directly reach the centre of the glaciated surface, which is approximatly 200 m from the moraine. Rough calculations of required reach angles for moraine-derived debris to reach the centreline on other glaciers in the catchment, based on the mean moraine prominence (Miles et al., 2017c), shows that this is likely true there as well. For the largest glacier, Langtang, the reach angle becomes 6°, while for the second largest, Langshisha, 18°. Due to differences in valley shape and moraine size, very different rates of relative coverage by moraine-derived debris are however possible. The runout length has increased over time as the glacier downwasted and the elevation range between the moraine crest and glacier tongue increased. The debris currently found at the glacier's centreline has either moved there by secondary processes such as glacier movement and on-glacier sliding, or originated from other sources, e.g. headwall erosion (Benn and Owen, 2002) or basal debris, (re-)emerging at the glacier surface towards the tongue (Boulton, 1978; Wirbel et al., 2018).

4.6 Clast analysis

The locations of the clast samples are shown in Figure 9. The C_{40} index is relatively low (0.2 to 0.48), while the rounded and very rounded fraction of the investigated is less than 6% on average, indicative of angular clasts. Looking at the angular and very angular fraction, the RA index, provides a stronger indication of transport processes (Figure 9). The RA index on the moraine is on average just above 30% suggesting a dominance in more rounded samples. This is due to their previous transport path through the ice before they were deposited along the moraine. Values are decreasing downglacier, corresponding to findings in Benn and Ballantyne (1994), indicating that englacially transported and moraine-derived debris becomes dominant. Higher RA indices on the moraine are found only where the moraine is still connected to the headwall (Figure 9). Clast samples in the centre of the glacier have a much higher RA index, >50%, as they have been dominantly sourced directly from headwalls further up-glacier, and less frequently emerged from englacial pathways. Clast samples from between the moraine and the

modelled runout length have an RA index higher than 50%, closer to the RA index of the samples in the centre of the glacier. This may indicate that the modelled runout length is an upper maximum and debris from the moraines rarely reaches this far, which is in line with the observed runout length being shorter.

4.7 Consequences for terminus retreat and debris thickness

Debris-covered tongues are schematized with a convex-concave up-glacier thickness pattern, causing lower tongues to be covered in thick debris that causes debris-covered tongues to stagnate (Anderson and Anderson, 2018; Watson et al., 2017; Kirkbride, 2000; Kirkbride and Deline, 2013). This can be explained with debris being accumulating continuously at the snout at higher rates than it can be evacuated (Figure 10A2). Moraine-derived debris can not be directly deposited over the complete width of the tongue (Figure 10A1), although secondary processes may be capable to further distribute it across the glacier. However, to get a first order estimate of its potential relative contribution to the thick cover expected on the snout, erosion rates from the moraines were compared to the overall debris thickness of the glacier. If it is assumed that all lateral moraine erosion (0.31 m yr^{-1} over an area of 0.18 km^2) is distributed equally over the entire glacier surface within the UAV domain (0.33 km^2), this results in an annual increase in debris thickness of 0.17 m. If the debris is only deposited within the area constrained by the maximum runout distance (192505 m^2) this implies an annual increase in debris thickness of 0.29 m. These estimated increases in debris thickness seem high given that the observed debris thickness for this glacier is in the range of 0.11 - 2.5 m (Ragettli et al., 2015; McCarthy et al., 2017). However a number of arguments make these rates plausible. (a) Direct measurements of debris thickness are few and generally from the centre of the glacier. It is very possible that debris is thicker along the base of the moraines. Furthermore, on the lower part of the Baltoro Glacier in the Karakoram similar debris accumulation rates have been found, ranging between 0.05 and 0.30 m yr^{-1}, suggesting that debris-covered tongues get buried rapidly (Gibson et al., 2017a). (b) Debris is evacuated from the surface via the glacier forefield, evidenced by regular rockfall and debris flows at the terminal ice cliffs observed in the field (Figure 10A4). We do not account for that in our balance and it could additionally lower the rate of increase in thickness. Hallet et al. (1996) and Gardner and Jones (1984) find erosion rates of approximately 5 mm yr^{-1} for one field site in the Karakoram, however empirical relations based on extensive measurements (Fenn et al., 1985; Hammer and Smith, 1982) suggest that based on the observed discharge rates between 0.75 m^3 s^{-1} in the dry and 2.25 m^3 s^{-1} in the wet season (Ragettli et al., 2015), evacuation rates for suspended sediments and bedload of 0.03 to 0.04 m yr^{-1} are possible. Of likely minor importance in total volume is evacuation of suspended sediments via aeolian transport. (c) The largest volume of relocated moraine debris is however likely due to slumping at the terminus (Figure 6A). As the tongue retreats, the debuttressing of the glacier causes the moraine to slump and fill the space available with moraine material (Figure 10A3 and B2). This is supported by the fact that observed rates in the upper part of the moraine (0.16 m yr^{-1}) correspond closely to observations in other regions (Ballantyne, 2002; Curry et al., 2006), while erosion at the lower moraine are twice as high (0.35 m yr^{-1}). At Lirung Glacier, the terminus retreated at a rate of 30 m yr^{-1} at the centreline and much slower at the margins as here the thick moraine-derived debris quickly covered the ice, resulting in the moraine crest to slump and become shallower (Figure 10B2). Along with internal ablation due to drainage conduits, this helps to explain the clear concave arcuate terminus appearance of retreating DCGs as opposed to the generally convex terminus of clean glaciers.

Considering these processes, the observations are plausible and show that lateral moraine erosion can play an major role in debris supply to downwasted glacier tongues with steep lateral moraines. This process could be an important negative feedback as the further a glacier downwastes the faster debris is supplied to its surface and the more melt is reduced. This is important to take into account in glacier flow and energy balance models (Carenzo et al., 2016; Anderson and Anderson, 2018; Rowan et al., 2015), which often use a uniform debris cover derived solely from headwall erosion and do not take lateral moraine debris supply into account.

5 Conclusion

In this study a time series of five years of UAV data is used to investigate the importance of lateral moraine erosion to a debris-covered tongue and the following key conclusions are drawn:

- The erosion from the lateral moraines is high at an average rate of 0.31 m yr^{-1} and this translates to an average increase of debris on the glacier tongue of 0.17 m yr^{-1}, ignoring sediment evacuation out of the glacier.
- For strongly downwasted glaciers with high and steep lateral moraines this could be an important negative feedback mechanisms as an increase in debris supply to the glacier tongue will suppress further melt of the tongue.
- There is a strong seasonality in lateral moraine erosion and the rates are higher in the wet season, which is indicative that water driven erosion is the key mechanism.
- The upper firm and steep part of the moraine is gullied and transports water quickly to the loose and gentle lower part where erosion occurs through water flow, debris entrainment and slow slumping. The slow slumping might be caused by solifluction for which the conditions are favorable.
- Rockfall and landslides occur occasionally and influence the erosional pattern, they are however of minor importance in the overall balance.
- Runout distance modelling shows that it is unlikely that these processes are responsible for the distribution of the eroded material on the glacier since the maximum distance are small (~56 m). This is supported by the clast analysis, which shows angularity to increase rapidly from the moraine (30% being angular or very angular) towards the glacier centre (>55% being angular or very angular).
- Further research is needed that incorporates glacier dynamics and lateral drag with the moraines and its implications for debris transport. In addition methods to quantify headwall erosion rates as well as subglacial erosion on debris-covered glaciers need to be developed to understand the full sediment balance of a debris-covered glacier tongue.

Author contributions. JS, PK, EM and WI developed the research goal. TW, JS and PK performed the primary data analysis and model development. TW, JS and WI wrote the manuscript. PK and EM helped with interpretation of results.

Competing interests. The authors declare no competing interests.

Acknowledgements. This project was supported by funding from the European Research Council (ERC) under the European Union's Horizon 2020 research and innovation program (grant agreement no. 676819) and by the research programme VIDI with project number 016.161.308 financed by the Netherlands Organisation for Scientific Research (NWO).

The input from Tjalling de Haas on erosional processes is also greatly appreciated.

References

Anderson, L. S. and Anderson, R. S.: Debris thickness patterns on debris-covered glaciers, Geomorphology, 311, 1–12, https://doi.org/10.1016/J.GEOMORPH.2018.03.014, 2018.

Ballantyne, C. K.: A general model of paraglacial landscape response, The Holocene, 12, 371–376, https://doi.org/10.1191/0959683602hl553fa, 2002.

Ballantyne, C. K. and Benn, D. I.: Paraglacial Slope Adjustment and Resedimentation Following Recent Glacier Retreat, Fabergstolsdalen, Norway, Arctic and Alpine Research, 26, 255–269, 1994.

Ballantyne, C. K. and Matthews, J. A.: The Development of sorted circles on recently deglaciated terrain, Jotunheinmen, Norway, Artic and Alpine Research, 14, 341–354, https://doi.org/Doi 10.2307/1550796, 1982.

Benn, D. I. and Ballantyne, C. K.: Reconstructing the transport history of glacigenic sediments: a new approach based on the co-variance of clast form indices, Sedimentary Geology, 91, 215–227, https://doi.org/10.1016/0037-0738(94)90130-9, 1994.

Benn, D. I. and Owen, L. A.: Himalayan glacial sedimentary environments: A framework for reconstructing and dating the former extent of glaciers in high mountains, Quaternary International, 97-98, 3–25, https://doi.org/10.1016/S1040-6182(02)00048-4, 2002.

Bolch, T., Kulkarni, A. V., Kääb, A., Huggel, C., Paul, F., Cogley, J. G., Frey, H., Kargel, J. S., Fujita, K., Scheel, M., Bajracharya, S., Stoffel, M., Kaab, A., Huggel, C., Paul, F., Cogley, J. G., Frey, H., Kargel, J. S., Fujita, K., Scheel, M., Bajracharya, S., and Stoffel, M.: The state and fate of Himalayan glaciers., Science, 336, 310–4, https://doi.org/10.1126/science.1215828, 2012.

Boulton, G. S.: Boulder shapes and grain-size distributions of debris as indicators of transport paths through a glacier and till genesis, Sedimentology, 25, 773–799, 1978.

Brun, F., Berthier, E., Wagnon, P., Kääb, A., and Treichler, D.: A spatially resolved estimate of High Mountain Asia glacier mass balances from 2000 to 2016, Nature Geoscience, 10, https://doi.org/10.1038/ngeo2999, 2017.

Cai, F. and Ugai, K.: Numerical Analysis of Rainfall Effects on Slope Stability, International Journal of Geomechanics, 4, 69–78, https://doi.org/10.1061/(ASCE)1532-3641(2004)4:2(69), 2004.

Carenzo, M., Pellicciotti, F., Mabillard, J., Reid, T., and Brock, B. W.: An enhanced debris temperature index model accounting for thickness effect, Advances in Water Resources, 94, 457–469, https://doi.org/10.1016/j.advwatres.2016.05.001, 2016.

Corominas, J., Copons, R., Vilaplana, J. M., Altimir, J., and Amigó, J.: Integrated Landslide Susceptibility Analysis and Hazard Assessment in the Principality of Andorra, Natural Hazards, 30, 421–435, 2003.

Curry, A. M., Cleasby, V., and Zukowskyj, P.: Paraglacial response of steep, sediment-mantled slopes to post-'Little Ice Age' glacier recession in the central Swiss Alps, Journal of Quaternary Science, 21, 211–225, https://doi.org/10.1002/jqs.954, 2006.

Dai, F. C. and Lee, C. F.: Landslide characteristics and slope instability modeling using GIS, Lantau Island, Hong Kong, Geomorphology, 42, 213–228, https://doi.org/10.1016/S0169-555X(01)00087-3, 2002.

De Haas, T., Braat, L., Leuven, J. R., Lokhorst, I. R., and Kleinhans, M. G.: Effects of debris flow composition on runout, depositional mechanisms, and deposit morphology in laboratory experiments, Journal of Geophysical Research F: Earth Surface, 120, 1949–1972, https://doi.org/10.1002/2015JF003525, 2015.

Deline, P.: Change in surface debris cover on Mont Blanc massif glaciers after the 'Little Ice Age' termination, The Holocene, 15, 302–309, https://doi.org/10.1191/0959683605hl809rr, 2005.

Deline, P., Gruber, S., Delaloye, R., Fischer, L., Geertsema, M., Giardino, M., Hasler, A., Kirkbride, M., Krautblatter, M., Magnin, F., McColl, S., Ravanel, L., and Schoeneich, P.: Ice Loss and Slope Stability in High-Mountain Regions, in: Snow and Ice-Related Hazards, Risks, and Disasters, pp. 521–561, Elsevier, https://doi.org/10.1016/B978-0-12-394849-6.00015-9, 2014.

Evans, S. and Hungr, O.: The assessment of rockfall hazard at the base of talus slopes, Canadian Geotechnical Journal, 30, 620–636, https://doi.org/10.1139/t93-054, 1993.

Fenn, C. R., Gurnell, A. M., and Beecroft, I. R.: An Evaluation of the Use of Suspended Sediment Rating Curves for the Prediction of Suspended Sediment Concentration in a Proglacial Stream, Source: Geografiska Annaler. Series A, Physical Geography, 672, 71–82, 1985.

Foster, L. A., Brock, B. W., Cutler, M. E. J., and Diotri, F.: A physically based method for estimating supraglacial debris thickness from thermal band remote-sensing data, Journal of Glaciology, 58, 677–691, https://doi.org/10.3189/2012JoG11J194, 2012.

Frauenfelder, R., Laustela, M., and Kääb, A.: Relative age dating of Alpine rockglacier surfaces, Zeitschrift Fur Geomorphologie, 49, 145–166, 2005.

Gardelle, J., Berthier, E., and Arnaud, Y.: Slight mass gain of Karakoram glaciers in the early twenty-first century, Nature Geoscience, 5, 322–325, https://doi.org/10.1038/ngeo1450, 2012.

Gardner, J. S. and Jones, N. K.: Sediment transport and yield at the Rakiot Glacier, Nanga Parbat, Punjab Himalaya., in: The International Karakoram Project 1, edited by K.J. Miller, pp. 184–197, Cambridge University Press, Cambridge, UK, 1984.

Gibson, M. J., Glasser, N. F., Quincey, D. J., Mayer, C., Rowan, A. V., and Irvine-Fynn, T. D.: Temporal variations in supraglacial debris distribution on Baltoro Glacier, Karakoram between 2001 and 2012, Geomorphology, 295, 572–585, https://doi.org/10.1016/j.geomorph.2017.08.012, 2017a.

Gibson, M. J., Glasser, N. F., Quincey, D. J., Rowan, A. V., Glasser, N. F., Quincey, D. J., and Rowan, A. V.: Changes in glacier surface cover on Baltoro glacier , Karakoram , North Pakistan , 2001 – 2012, Journal of Maps, 5647, https://doi.org/10.1080/17445647.2016.1264319, 2017b.

Gruber, S., Fleiner, R., Guegan, E., Panday, P., Schmid, M.-O., Stumm, D., Wester, P., Zhang, Y., and Zhao, L.: Review article: Inferring permafrost and permafrost thaw in the mountains of the Hindu Kush Himalaya region, The Cryosphere, 11, 81–99, https://doi.org/10.5194/tc-11-81-2017, 2017.

Hallet, B., Hunter, L., and Bogen, J.: Rates of erosion and sediment evacuation by glaciers: A review of field data and their implications, Global and Planetary Change, 12, 213–235, 1996.

Hammer, K. M. and Smith, N. D.: Sediment Production and Transport in a Proglacial Stream: Hilda Glacier, Alberta, Canada, Boreas, 12, 91–106, 1982.

Heimsath, A. M. and McGlynn, R.: Quantifying periglacial erosion in the Nepal high Himalaya, Geomorphology, 97, 5–23, https://doi.org/10.1016/j.geomorph.2007.02.046, 2008.

Herreid, S., Pellicciotti, F., Ayala, A., Chesnokova, A., Kienholz, C., Shea, J., and Shrestha, A.: Satellite observations show no net change in the percentage of supraglacial debris-covered area in northern Pakistan from 1977 to 2014, Journal of Glaciology, 61, 524–536, https://doi.org/10.3189/2015JoG14J227, 2015.

Immerzeel, W. W., van Beek, L. P. H., and Bierkens, M. F. P.: Climate Change Will Affect the Asian Water Towers, Science, 328, 1382–1385, https://doi.org/10.1126/science.1183188, 2010.

Immerzeel, W. W., Kraaijenbrink, P., Shea, J. M., Shrestha, A. B., Pellicciotti, F., Bierkens, M. F. P., and de Jong, S. M.: High-resolution monitoring of Himalayan glacier dynamics using unmanned aerial vehicles, Remote Sensing of Environment, 150, 93–103, https://doi.org/10.1016/j.rse.2014.04.025, 2014a.

Immerzeel, W. W., Petersen, L., Ragettli, S., and Pellicciotti, F.: The importance of observed gradients of air temperature and precipitation for modeling runoff from a glacierized watershed in the Nepalese Himalayas, Water Resources Research, 50, 2212–2226, https://doi.org/10.1002/2013WR014506, 2014b.

Iverson, R. M.: The physics of debris flows, Reviews of Geophysics, 35, 245–296, https://doi.org/10.1029/97RG00426, 1997.

Kääb, A., Berthier, E., Nuth, C., Gardelle, J., and Arnaud, Y.: Contrasting patterns of early twenty-first-century glacier mass change in the Himalayas., Nature, 488, 495–8, https://doi.org/10.1038/nature11324, 2012.

Kirkbride, M. M. P.: Ice-marginal geomorphology and Holocene expansion of debris-covered Tasman Glacier, New Zealand, IAHS publication, pp. 211–217, 2000.

Kirkbride, M. P. and Deline, P.: The formation of supraglacial debris covers by primary dispersal from transverse englacial debris bands, Earth Surface Processes and Landforms, 38, 1779–1792, https://doi.org/10.1002/esp.3416, 2013.

Kirkby, M. J.: Measurement and Theory of Soil Creep, The Journal of Geology, 75, 359–378, https://doi.org/10.1086/627267, 1967.

Kraaijenbrink, P. D. A., Meijer, S. W., Shea, J. M., Pellicciotti, F., Jong, S. M. D. E., and Immerzeel, W. W.: Seasonal surface velocities of a Himalayan glacier derived by automated correlation of unmanned aerial vehicle imagery, Annals of Glaciology, 57, 103–113, https://doi.org/10.3189/2016AoG71A072, 2016.

Kraaijenbrink, P. D. A., Bierkens, M. F. P., Lutz, A. F., and Immerzeel, W. W.: Impact of a global temperature rise of 1.5 degrees Celsius on Asia's glaciers, Nature, 549, 257–260, https://doi.org/10.1038/nature23878, 2017.

Leprince, S., Ayoub, F., Klinger, Y., and Avouac, J.-P.: Co-Registration of Optically Sensed Images and Correlation (COSI-Corr): an operational methodology for ground deformation measurements, in: 2007 IEEE International Geoscience and Remote Sensing Symposium, pp. 1943–1946, IEEE, https://doi.org/10.1109/IGARSS.2007.4423207, 2007.

Lukas, S., Graf, A., Coray, S., and Schlüchter, C.: Genesis, stability and preservation potential of large lateral moraines of Alpine valley glaciers - towards a unifying theory based on Findelengletscher, Switzerland, Quaternary Science Reviews, 38, 27–48, https://doi.org/10.1016/j.quascirev.2012.01.022, 2012.

Lukas, S., Benn, D. I., Boston, C. M., Brook, M., Coray, S., Evans, D. J., Graf, A., Kellerer-Pirklbauer, A., Kirkbride, M. P., Krabbendam, M., Lovell, H., Machiedo, M., Mills, S. C., Nye, K., Reinardy, B. T., Ross, F. H., and Signer, M.: Clast shape analysis and clast transport paths in glacial environments: A critical review of methods and the role of lithology, Earth-Science Reviews, 121, 96–116, https://doi.org/10.1016/j.earscirev.2013.02.005, 2013.

Macfarlane, A. M., Hodges, K. V., and Lux, D.: A structural analysis of the Main Central Thrust zone, Langtang National Park, central Nepal Himalaya, Geological Society of America Bulletin, 104, 1389–1402, 1992.

Matsuoka, N.: Solifluction rates, processes and landforms: A global review, Earth-Science Reviews, 55, 107–134, https://doi.org/10.1016/S0012-8252(01)00057-5, 2001.

McCarthy, M., Pritchard, H., Willis, I., and King, E.: Ground-penetrating radar measurements of debris thickness on Lirung Glacier, Nepal, Journal of Glaciology, 63, 543–555, https://doi.org/10.1017/jog.2017.18, 2017.

Mihalcea, C., Mayer, C., Diolaiuti, G., Lambrecht, A., Smiraglia, C., and Tartari, G.: Ice ablation and meteorological conditions on the debris-covered area of Baltoro glacier, Karakoram, Pakistan, Annals of Glaciology, 43, 292–300, https://doi.org/10.3189/172756406781812104, 2006.

Mihalcea, C., Brock, B. W., Diolaiuti, G., Agata, C. D., and Citterio, M.: Using ASTER satellite and ground-based surface temperature measurements to derive supraglacial debris cover and thickness patterns on Miage Glacier (Mont Blanc Massif , Italy), Cold Regions Science and Technology, 52, 341–354, https://doi.org/10.1016/j.coldregions.2007.03.004, 2008.

Miles, E. S., Steiner, J., Willis, I. C., Buri, P., Immerzeel, W. W., Chesnokova, A., and Pellicciotti, F.: Pond dynamics and supraglacial-englacial connectivity on debris-covered Lirung Glacier, Frontiers in Earth Science, 5, https://doi.org/10.3389/FEART.2017.00069, 2017a.

Miles, E. S., Steiner, J. F., and Brun, F.: Highly variable aerodynamic roughness length (z 0) for a hummocky debris-covered glacier, Journal of Geophysical Research: Atmospheres, 122, 1–20, https://doi.org/10.1002/2017JD026510, 2017b.

Miles, E. S., Willis, I. C., Arnold, N. S., Steiner, J. F., and Pellicciotti, F.: Spatial, seasonal, and interannual variability of supraglacial ponds in the Langtang Valley of Nepal, 1999 to 2013, Journal of Glaciology, 63, 88–105, https://doi.org/10.1017/jog.2016.120, 2017c.

Nicholson, L. and Benn, D.: Calculating ice melt beneath a debris layer using meteorological data, Journal of Glaciology, 52, 463–470, https://doi.org/10.3189/172756506781828584, 2006.

Nield, J. M., Chiverrell, R. C., Darby, S. E., Leyland, J., Vircavs, L. H., and Jacobs, B.: Complex spatial feedbacks of tephra redistribution, ice melt and surface roughness modulate ablation on tephra covered glaciers, Earth Surface Processes and Landforms, 38, 95–102, https://doi.org/10.1002/esp.3352, 2013.

Nuimura, T., Fujita, K., and Sakai, A.: Downwasting of the debris-covered area of Lirung Glacier in Langtang Valley, Nepal Himalaya, from 1974 to 2010, Quaternary International, 455, 93–101, https://doi.org/10.1016/J.QUAINT.2017.06.066, 2017.

Østrem, G.: Ice Melting under a Thin Layer of Moraine, and the Existence of Ice Cores in Moraine Ridges, Geografiska Annaler, 41, 228–230, 1959.

Pfeffer, W. T., Arendt, A. a., Bliss, A., Bolch, T., Cogley, J. G., Gardner, A. S., Hagen, J.-O., Hock, R., Kaser, G., Kienholz, C., Miles, E. S., Moholdt, G., Mölg, N., Paul, F., Radić, V., Rastner, P., Raup, B. H., Rich, J., Sharp, M. J., and The Randolph Consortium: The Randolph Glacier Inventory: a globally complete inventory of glaciers, Journal of Glaciology, 60, 537–552, https://doi.org/10.3189/2014JoG13J176, 2014.

Powers, M. C.: A new roundness scale for sedimentary particles, Journal of Sedimentary Petrology, 23, 1953.

Ragettli, S., Pellicciotti, F., Immerzeel, W. W., Miles, E. S., Petersen, L., Heynen, M., Shea, J. M., Stumm, D., Joshi, S., and Shrestha, A.: Unraveling the hydrology of a Himalayan catchment through integration of high resolution in situ data and remote sensing with an advanced simulation model, Advances in Water Resources, 78, 94–111, https://doi.org/10.1016/j.advwatres.2015.01.013, 2015.

Reheis, M. J.: Source, transportation and deposition of debris on Arapaho Glacier, Front Range, Colorado, U.S.A., Journal of Glaciology, 14, 1975.

Rickenmann, D.: Runout prediction methods, in: Debris-flow Hazards and Related Phenomena, edited by Jakob, M. and Hungr, O., chap. 13, pp. 305–324, Springer Berlin Heidelberg, Berlin, https://doi.org/10.1007/3-540-27129-5_13, 2005.

Römkens, M. J. M., Helming, K., and Prasad, S. N.: Soil erosion under different rainfall intensities, surface roughness, and soil water regimes, in: Catena, vol. 46, pp. 103–123, Elsevier, https://doi.org/10.1016/S0341-8162(01)00161-8, 2002.

Rounce, D. R. and McKinney, D. C.: Debris thickness of glaciers in the Everest Area (Nepal Himalaya) derived from satellite imagery using a nonlinear energy balance model, The Cryosphere, 8, 1317–1329, https://doi.org/10.5194/tcd-8-887-2014, 2014.

Rounce, D. R., King, O., McCarthy, M., Shean, D. E., and Salerno, F.: Quantifying Debris Thickness of Debris-Covered Glaciers in the Everest Region of Nepal Through Inversion of a Subdebris Melt Model, Journal of Geophysical Research: Earth Surface, 123, 1094–1115, https://doi.org/10.1029/2017JF004395, 2018.

Rowan, A. V., Egholm, D. L., Quincey, D. J., and Glasser, N. F.: Modelling the feedbacks between mass balance , ice flow and debris transport to predict the response to climate change of debris-covered glaciers in the Himalaya, Earth and Planetary Science Letters, 430, 427–438, https://doi.org/10.1016/j.epsl.2015.09.004, 2015.

Schauwecker, S., Rohrer, M., Huggel, C., Kulkarni, A., Ramanathan, A. L., Salzmann, N., Stoffel, M., and Brock, B.: Remotely sensed debris thickness mapping of Bara Shigri Glacier, Indian Himalaya, Journal of Glaciology, 61, 675–688, https://doi.org/10.3189/2015JoG14J102, 2015.

Scherler, D., Bookhagen, B., and Strecker, M. R.: Spatially variable response of Himalayan glaciers to climate change affected by debris cover, Nature Geoscience, 4, 156–159, https://doi.org/10.1038/ngeo1068, 2011.

Shukla, A., Gupta, R., and Arora, M.: Estimation of debris cover and its temporal variation using optical satellite sensor data: a case study in Chenab basin, Himalaya, Journal of Glaciology, 55, 444–452, https://doi.org/10.3189/002214309788816632, 2009.

Soldati, M., Corsini, A., and Pasuto, A.: Landslides and climate change in the Italian Dolomites since the Late glacial, CATENA, 55, 141–161, https://doi.org/10.1016/S0341-8162(03)00113-9, 2004.

Steiner, J. F., Pellicciotti, F., Buri, P., Miles, E. S., Immerzeel, W. W., and Reid, T. D.: Modelling ice-cliff backwasting on a debris-covered glacier in the Nepalese Himalaya, Journal of Glaciology, 61, 889–907, https://doi.org/10.3189/2015JoG14J194, 2015.

Stokes, C. R., Popovnin, V., Aleynikov, A., Gurney, S. D., and Shahgedanova, M.: Recent glacier retreat in the Caucasus Mountains, Russia, and associated increase in supraglacial debris cover and supra- / proglacial lake development, Annals of Glaciology, 46, 195–203, https://doi.org/http://dx.doi.org/10.3189/172756407782871468, 2007.

Thompson, S., Benn, D. I., Mertes, J., and Luckman, A.: Stagnation and mass loss on a Himalayan debris-covered glacier: processes, patterns and rates, Journal of Glaciology, c, 1–19, https://doi.org/10.1017/jog.2016.37, 2016.

van Rijn, L. C.: Sediment Transport, Part I: Bed Load Transport, Journal of Hydraulic Engineering, 110, 1431–1456, https://doi.org/10.1061/(ASCE)0733-9429(1984)110:10(1431), 1984.

Watanabe, T., Dali, L., and Shiraiwa, T.: Slope denudation and the supply of debris to cones in Langtang Himal, Central Nepal Himalaya, Geomorphology, 26, 185–197, https://doi.org/10.1016/S0169-555X(98)00058-0, 1998.

Watson, C., Quincey, D., Carrivick, J., and Smith, M.: Ice cliff dynamics in the Everest region of the Central Himalaya, Geomorphology, 142, 14–27, https://doi.org/10.1016/j.gloplacha.2016.04.008, 2017.

Wirbel, A., Jarosch, A. H., and Nicholson, L.: Modelling debris transport within glaciers by advection in a full-Stokes ice flow model, The Cryosphere, 12, 189–204, https://doi.org/10.5194/tc-12-189-2018, 2018.

Earth Surf. Dynam. Discuss., https://doi.org/10.5194/esurf-2018-63
Manuscript under review for journal Earth Surf. Dynam.
Discussion started: 11 September 2018

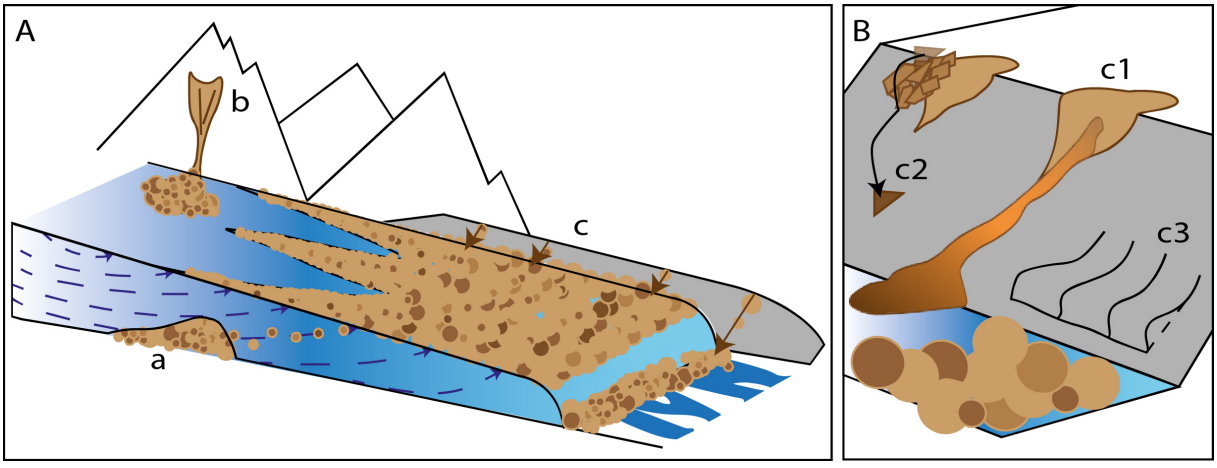

Figure 1. Schematization of debris supply processes towards the glacier surface (A), showing basal erosion (a), headwall erosion (b) and sediment supply from lateral moraines (c). Erosion on a lateral moraine bordering the glacier (B), showing debris flows (c1), rockfall (c2) and solifluction (c3).

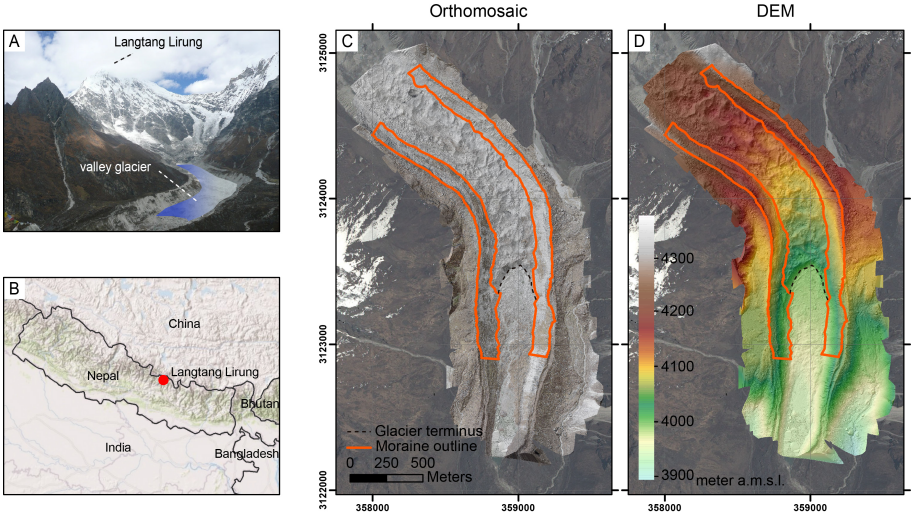

Figure 2. Study area including the setting (A), location of the study area (B) and two more detailed overviews including the orthomosaic and elevation data of the study area (C,D; from UAV flights in October 2015). The glacier terminus and studied section of the moraine are outlined on these maps.

Earth Surf. Dynam. Discuss., https://doi.org/10.5194/esurf-2018-63
Manuscript under review for journal Earth Surf. Dynam.
Discussion started: 11 September 2018

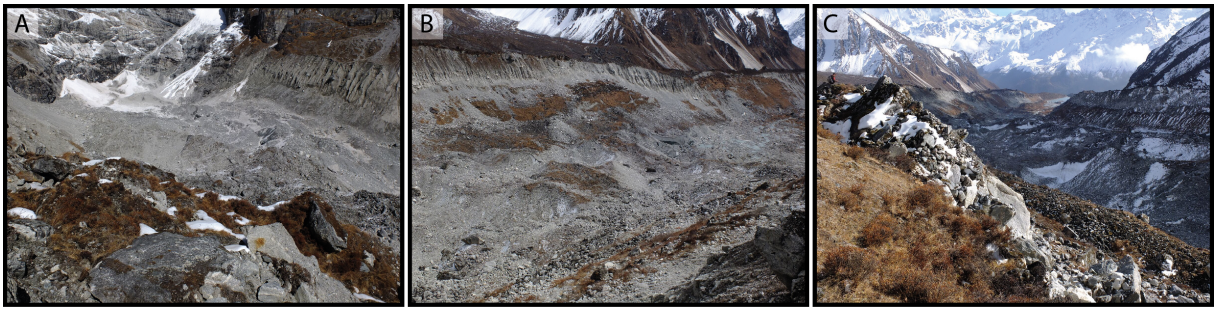

Figure 3. Field images of Lirung glacier from the upper part (A), where the headwalls are still connected to the glacier, along the middle disconnected part (B) to the lower glacier tongue (C), where the decoupling is clearly visible. Also note the mass movements from the upper slopes (B) that do not reach the glacier.

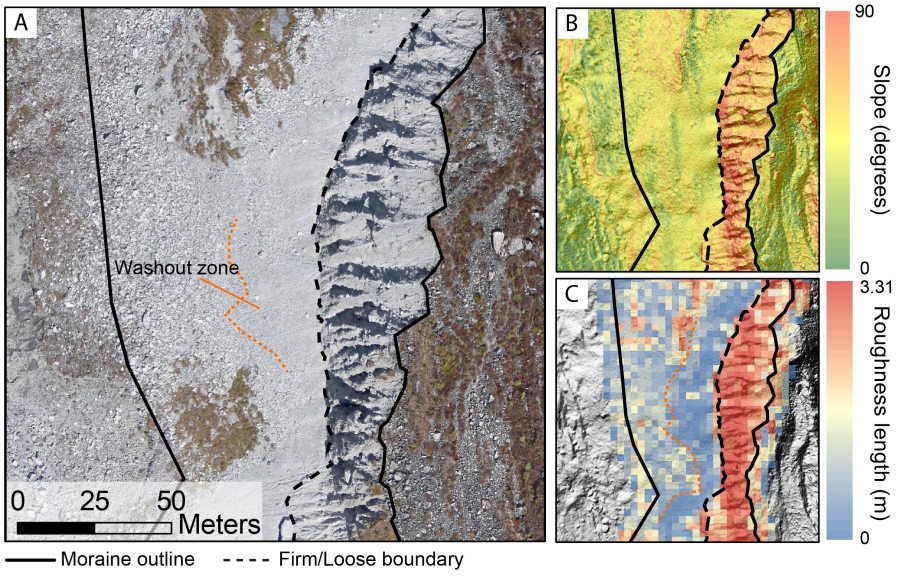

Figure 4. Moraine delineation method. The crest is often well defined by the orthomosaic (A) and slope (B). An intermediate washout zone is clearly visible from the roughness data (C). The intensely gullied upper part (right) is referred to as firm, the lower (left) part is referred to as loose.

Earth Surf. Dynam. Discuss., https://doi.org/10.5194/esurf-2018-63
Manuscript under review for journal Earth Surf. Dynam.
Discussion started: 11 September 2018

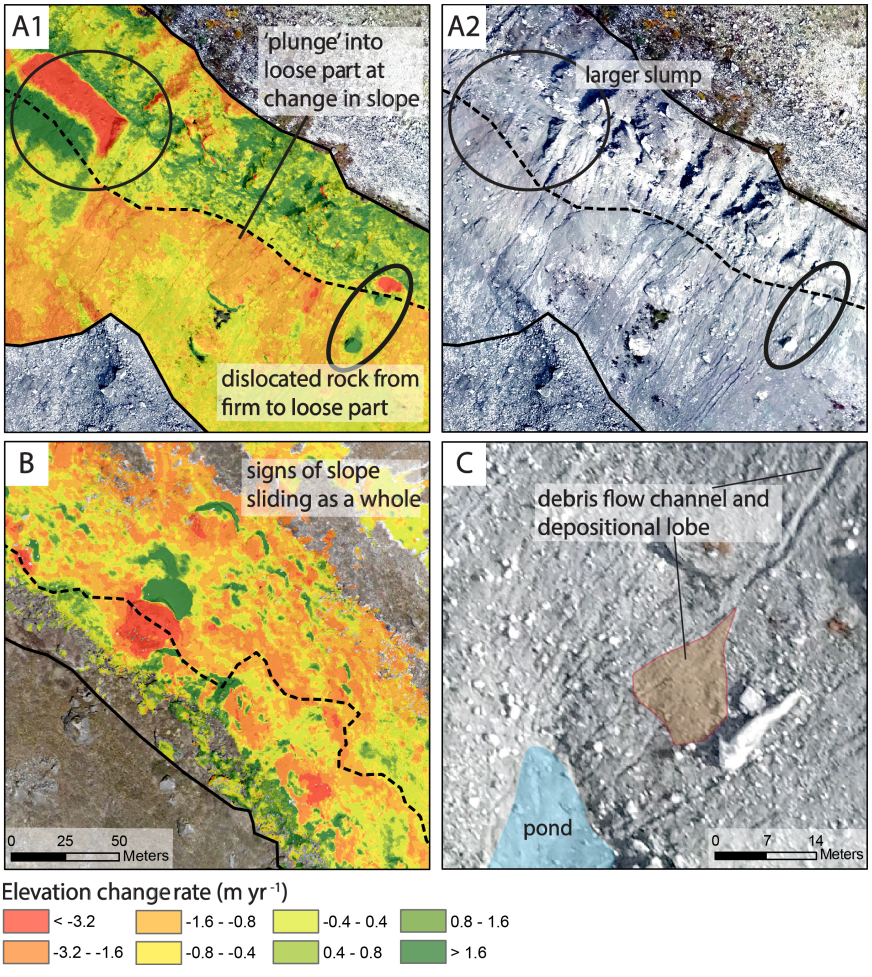

Figure 5. Different types or erosional mechanisms. Fast mass movements as slumps and rockfall occur on the moraine (A1, A2) as well as water driven movement as water flow and debris flows (C). Furthermore the slopes are slumping down slowly (B), which is clearly visible by the alternation of positive (rocks moving in) and negative (rocks moving out) elevation change values.

Earth Surf. Dynam. Discuss., https://doi.org/10.5194/esurf-2018-63
Manuscript under review for journal Earth Surf. Dynam.
Discussion started: 11 September 2018

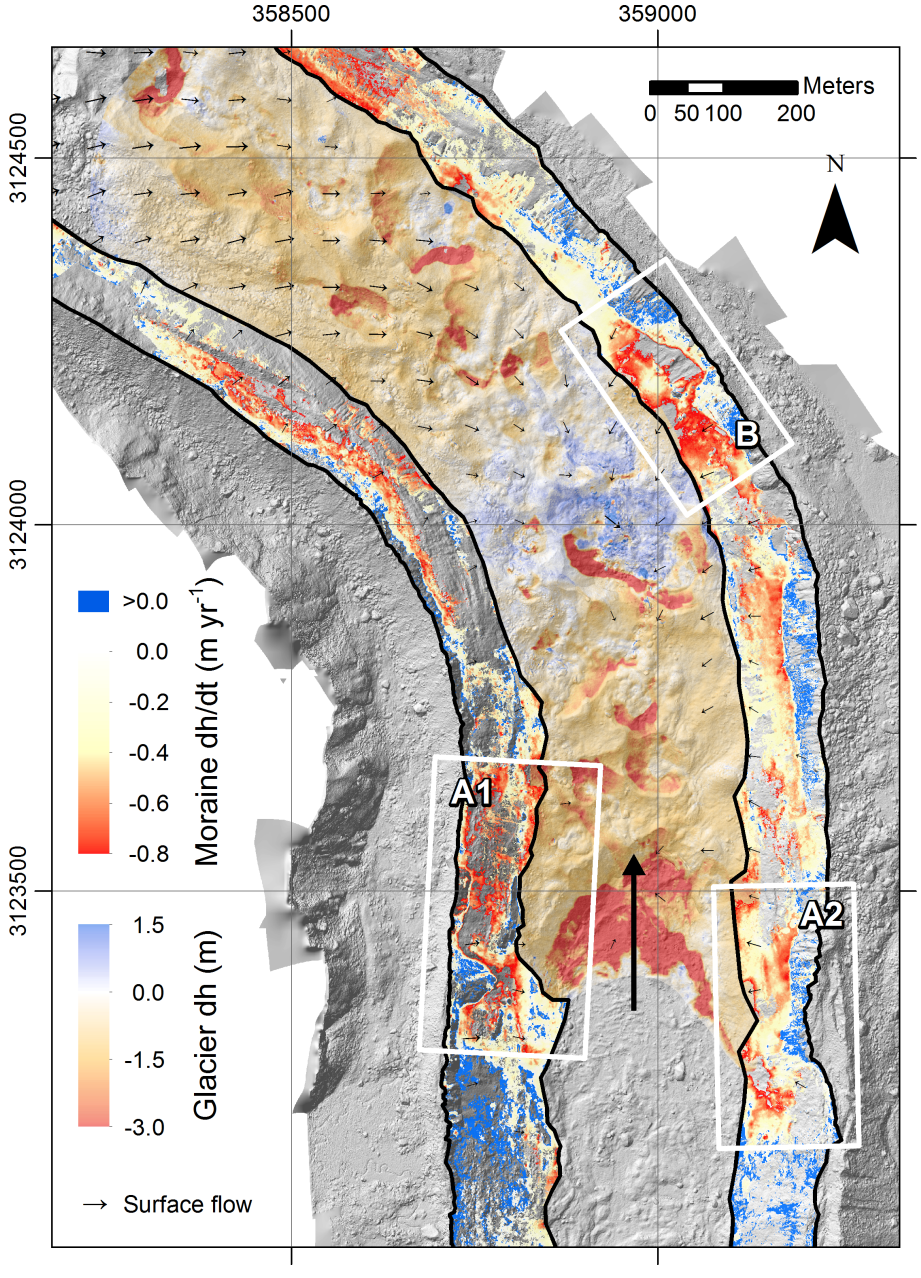

Figure 6. Downwasting of the glacier surface between May and October 2013 (Immerzeel et al., 2014a) as well as velocities (Kraaijenbrink et al., 2016) compared to erosion on the moraines. Insets A and B show hotspots of erosion. The long black arrow shows retreat of the terminus between 2013 and 2018 (~150 m).

Earth Surf. Dynam. Discuss., https://doi.org/10.5194/esurf-2018-63
Manuscript under review for journal Earth Surf. Dynam.
Discussion started: 11 September 2018

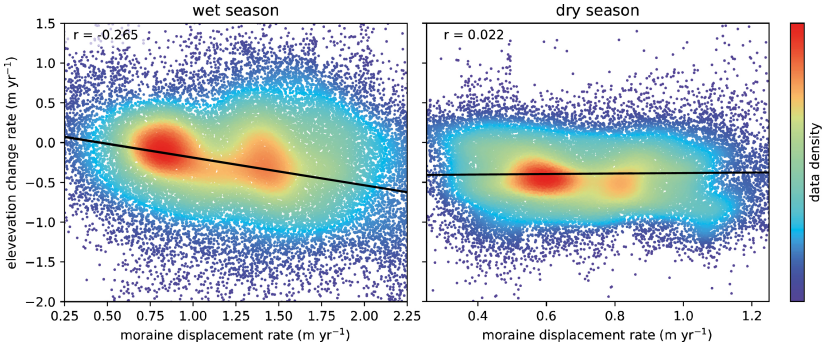

Figure 7. Relation between elevation change and moraine velocity in the wet and dry season. In the wet season, high velocities occur with higher erosion rates. No such relation exists in the dry season.

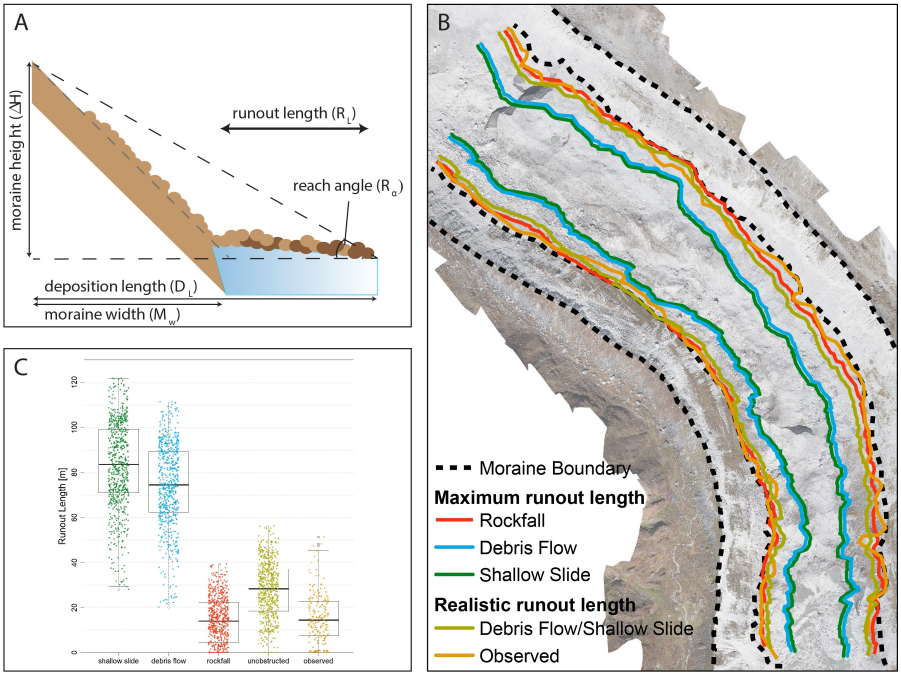

Figure 8. Conceptual diagram of model approach (Panel A), the modelled runout lengths (Panel B) and the modelled variability in runout lengths (Panel C).

Earth Surf. Dynam. Discuss., https://doi.org/10.5194/esurf-2018-63
Manuscript under review for journal Earth Surf. Dynam.
Discussion started: 11 September 2018

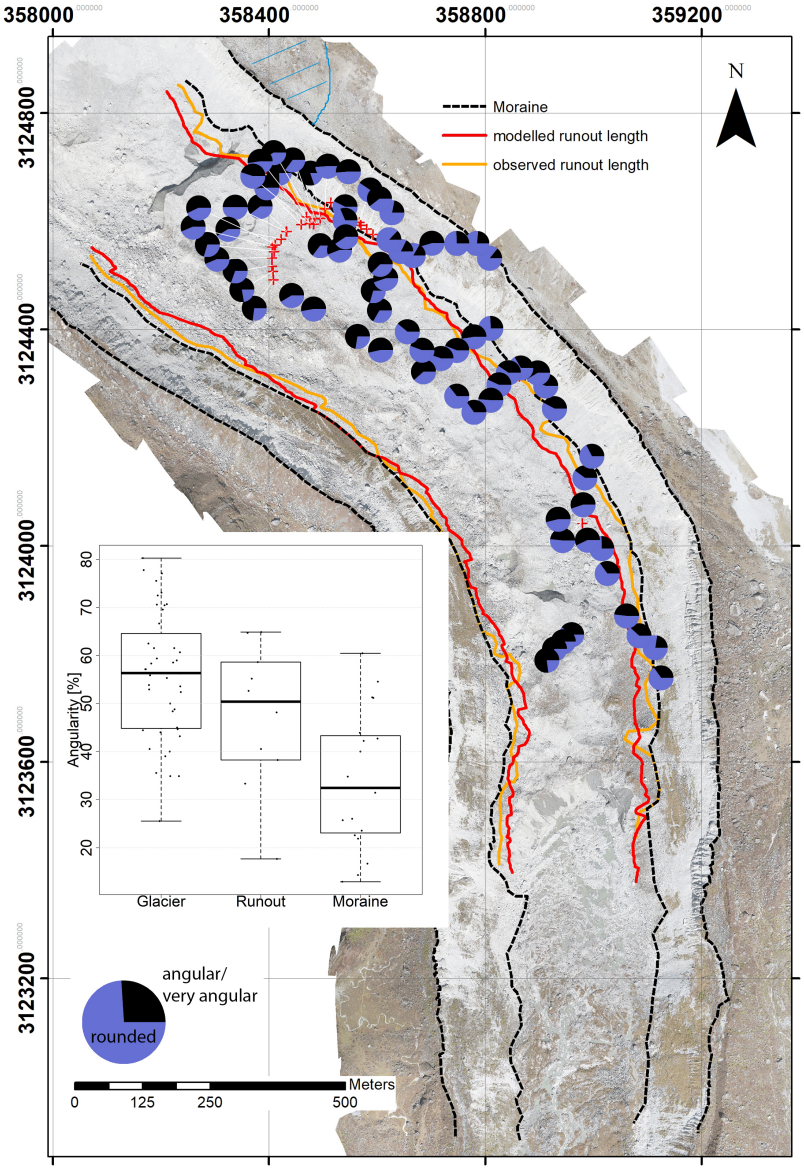

Figure 9. Angularity samples taken on the glacier surface, observed and modelled runout lengths are also shown. The inset shows angularity values for samples beyond the modelled runout length ('Glacier'), between the runout length and the base of the moraine ('Runout') and on the moraine ('Moraine'). In the top right corner, marked in blue, the glacier is still connected to headwalls by way of avalanching.

Earth Surf. Dynam. Discuss., https://doi.org/10.5194/esurf-2018-63
Manuscript under review for journal Earth Surf. Dynam.
Discussion started: 11 September 2018

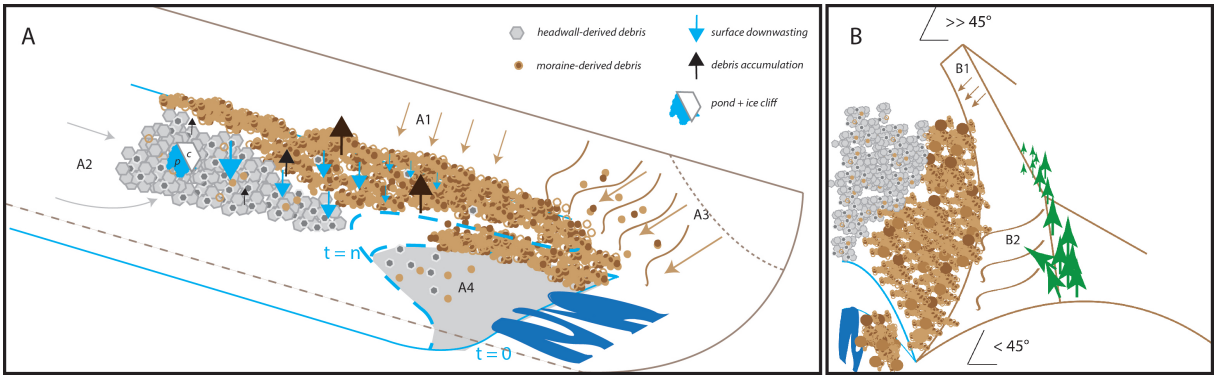

Figure 10. Dominant processes at lateral moraines and consequences for the glacier terminus of a debris covered glacier. Erosion from lateral moraines (A1) as well as debris transport from head walls and englacial transport (A2) are shown. Slumping as a consequence of debuttressing at the terminus (A3) brings more material into the glacier forefield (A4), as the tongue retreats in time (t). As a consequence the moraine crest slumps (B2) and the moraine becomes shallower compared to upper parts where transport is mainly to rockfall and debris flows (B1).

Table 1. Date of acquisition and area of the different datasets.

Date	mapped area [km^2]
2013 / 05 / 18	2.04
2013 / 10 / 22	3.25
2015 / 10 / 18	2.61
2016 / 04 / 30	1.97
2016 / 10 / 06	2.70
2017 / 04 / 20	1.41
2017 / 10 / 19	2.32
2018 / 04 / 28	2.12

Table 2. Extreme values below and above which the data is removed from the original dataset, as well as the mean of the whole dataset (μ).

Dataset	10^{th} percentile [m]	μ [m]	90^{th} percentile [m]
2013 / 05 - 2013 / 10 (wet)	-0.39	-2.07	1.18
2015 / 10 - 2016 / 04 (dry)	-0.17	-1.06	0.72
2016 / 04 - 2016 / 10 (wet)	-0.34	-1.47	0.87
2016 / 10 - 2017 / 04 (dry)	-0.36	-1.11	0.37
2017 / 04 - 2017 / 10 (wet)	-0.52	-2.16	1.11
2017 / 10 - 2018 / 04 (dry)	-0.22	-0.88	0.13
2013 / 05 - 2018 / 04 (total)	-0.31	-1.94	1.97

Earth Surf. Dynam. Discuss., https://doi.org/10.5194/esurf-2018-63
Manuscript under review for journal Earth Surf. Dynam.
Discussion started: 11 September 2018

Earth Surface Dynamics Discussions Open Access EGU

Table 3. Seasonal elevation change values, furthermore divided in upper and loose moraine. All erosion values are in meters. Precipitation is measured at Kyanjing station in 2013 and Langshisha station in all others easons.

	Entire moraine		Firm, upper part		Loose, lower part		Precipitation	
Dataset	μ	σ	μ	σ	μ	σ	cumulative [mm]	mean intensity [mm h^{-1}]
2013 / 05 - 2013 / 10 (wet)	0.39	0.79	0.28	0.77	0.41	0.83	697	0.90
2015 / 10 - 2016 / 04 (dry)	0.17	0.44	0.07	0.43	0.21	0.44	145	0.62
2016 / 04 - 2016 / 10 (wet)	0.34	0.57	0.14	0.55	0.41	0.59	584	0.58
2016 / 10 - 2017 / 04 (dry)	0.36	0.37	0.24	0.37	0.41	0.36	172	0.84
2017 / 04 - 2017 / 10 (wet)	0.52	0.84	0.19	0.82	0.60	0.82	541	0.58
2017 / 10 - 2018 / 04 (dry)	0.22	0.98	0.12	0.98	0.25	1.00	117	0.50
2013 / 05 - 2018 / 04 (total)	0.31	0.26	0.16	0.26	0.41	0.21	2257	0.67